Energy & Environmental Science

Supporting Information

Constructing van der Waals Gaps in Cubic-structured SnTe-based Thermoelectric Materials

Xiao Xu[1,#], Juan Cui[1,#], Yong Yu[1,#], Bin Zhu[1], Yi Huang[1], Lin Xie[1], Di Wu[2] and Jiaqing He[1,*]

[1]Department of physics, Southern University of Science and Technology, Shenzhen, 518055, China.

[2]School of Materials Science and Engineering, Shaanxi Normal University, Xi'an, 710119, China.

[#]These authors contributed equally

*Correspondence: he.jq@sustc.edu.cn

Figures

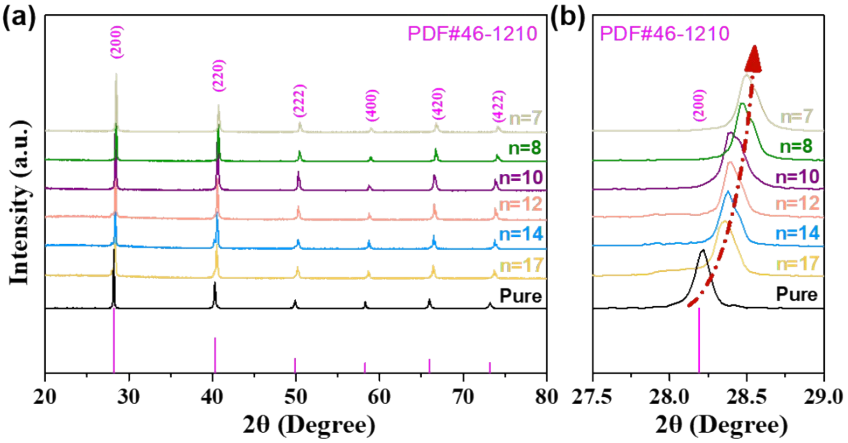

Figure S1. (a) XRD pattern and (b) the magnified XRD pattern of $Sb_2Te_3(SnTe)_n$ samples.

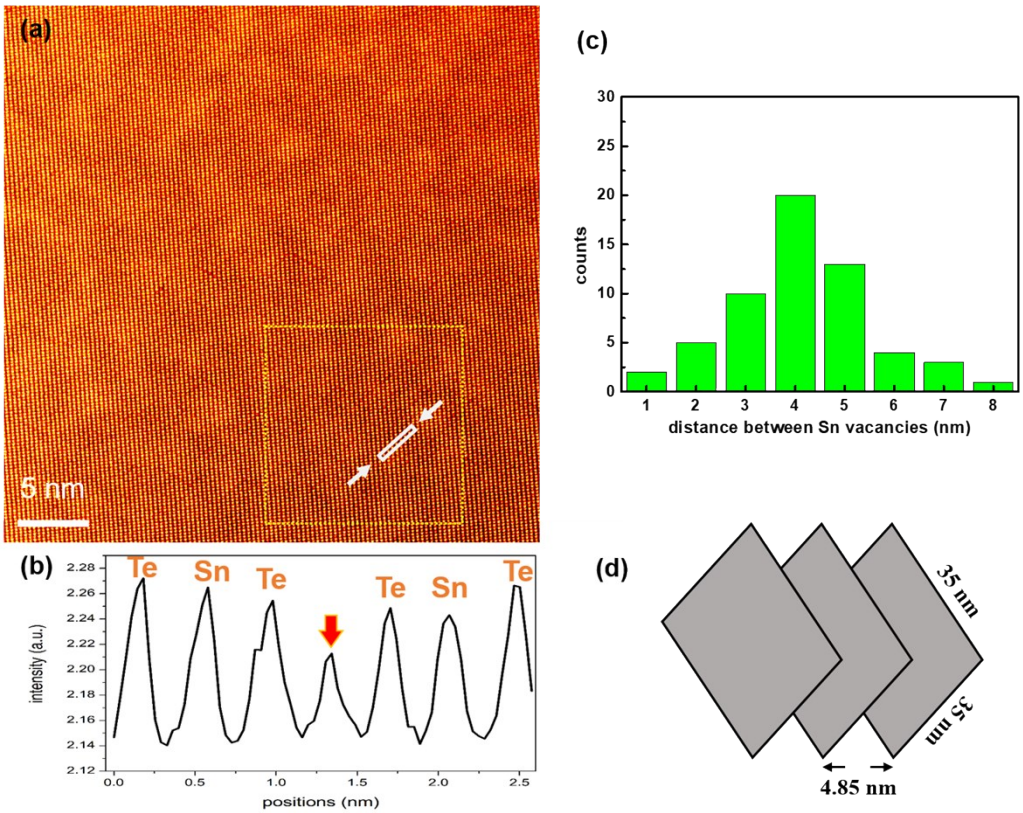

Figure S2. (a) The false-color HAADF-STEM image of $Sb_2Te_3(SnTe)_8$ sample, (b) the atomic line scanning profile of corresponding area, (c) the statistical data of the distance between Sn vacancies, and (d) the schematic diagrams of characteristic length between two gaps in an area of 35×35 nm^2.

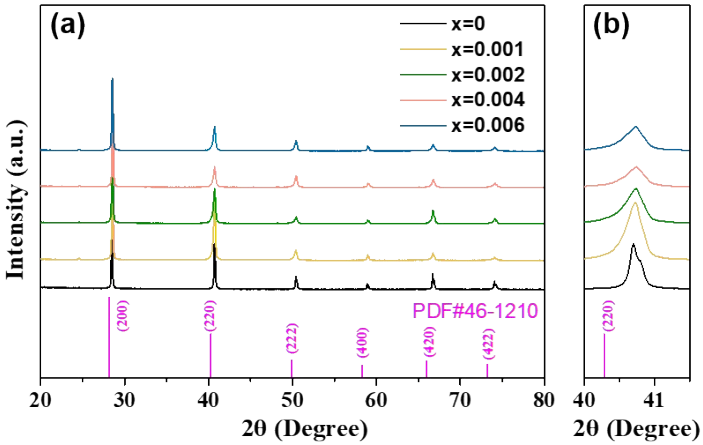

Figure S3. (a) XRD pattern and (b) the magnified XRD pattern of the $Sb_2Te_3(Sn_{1-x}Re_xTe)_n$ samples.

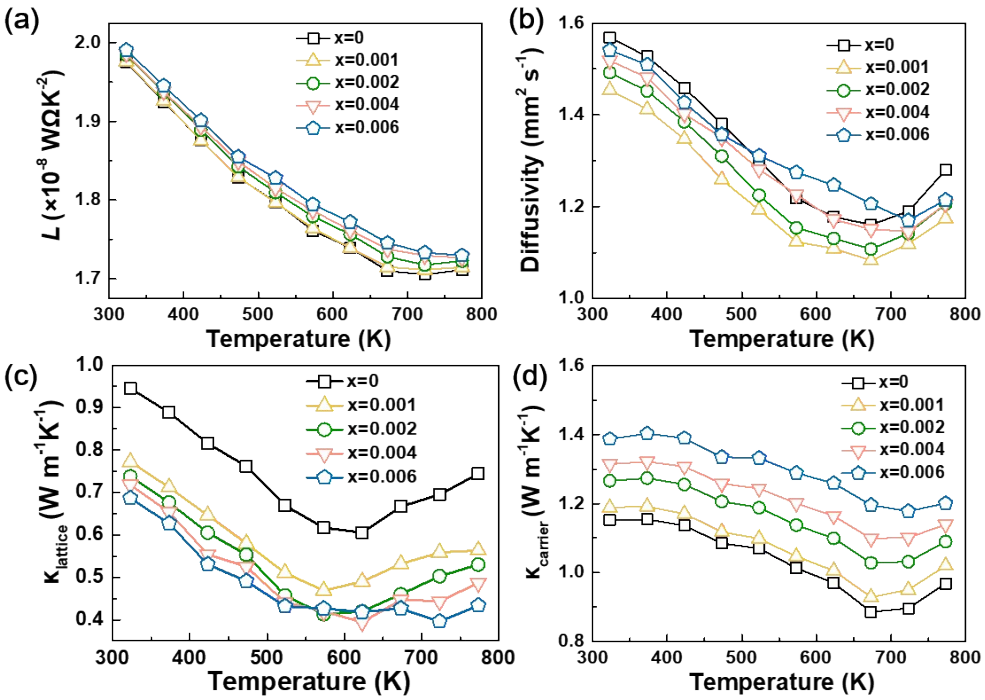

Figure S4. The temperature dependence of (a) Lorenz number, (b) diffusivity, (c) lattice thermal conductivity, and (d)carrier thermal conductivity of $Sb_2Te_3(Sn_{1-x}Re_xTe)_n$ samples.

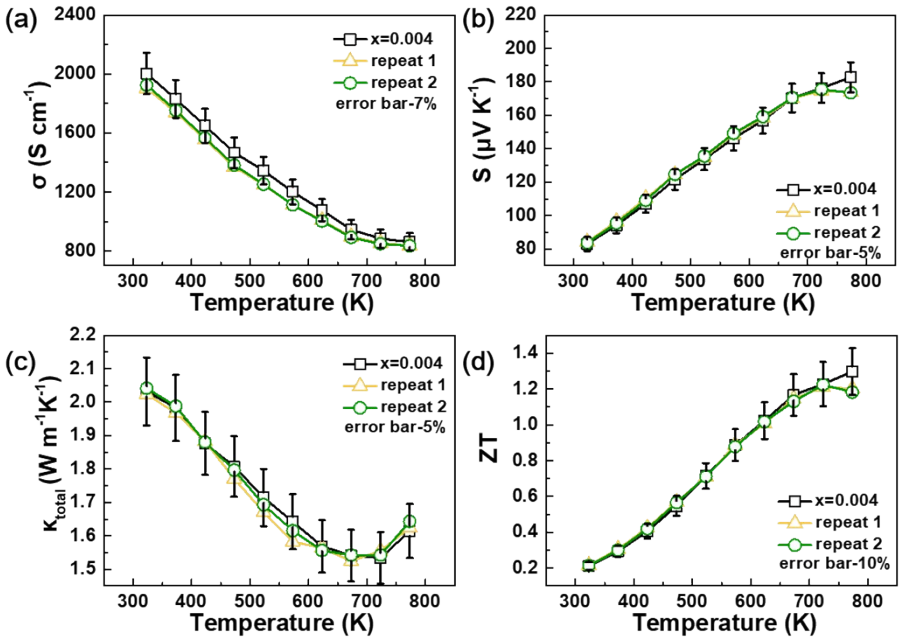

Figure S5. The repeatability test of the $Sb_2Te_3(Sn_{0.996}Re_{0.004}Te)_8$ sample. The temperature dependence of (a) electrical conductivity, (b) Seebeck coefficient, (c) total thermal conductivity, and (d) *ZT* value.

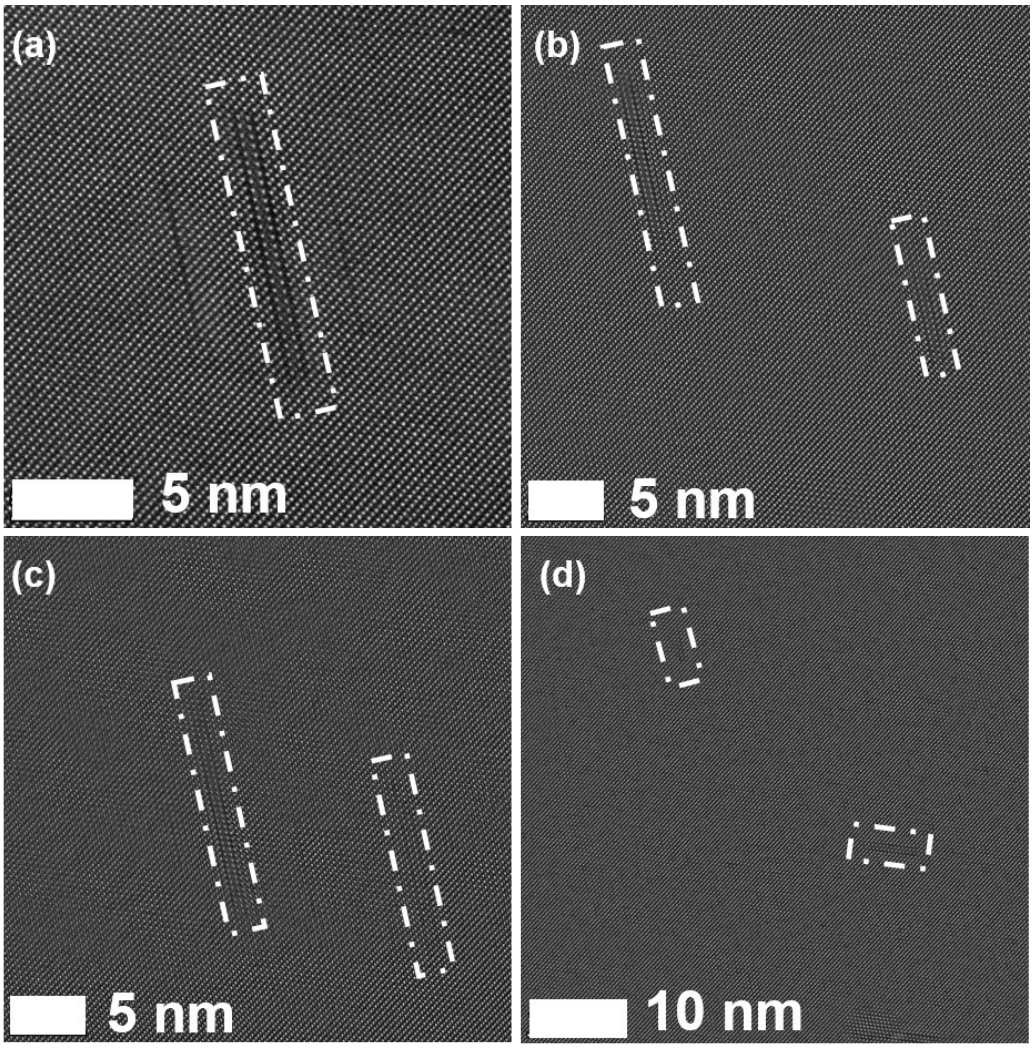

Figure S6. The high magnified STEM-HAADF images of $Sb_2Te_3(Sn_{0.996}Re_{0.004}Te)_8$ sample.

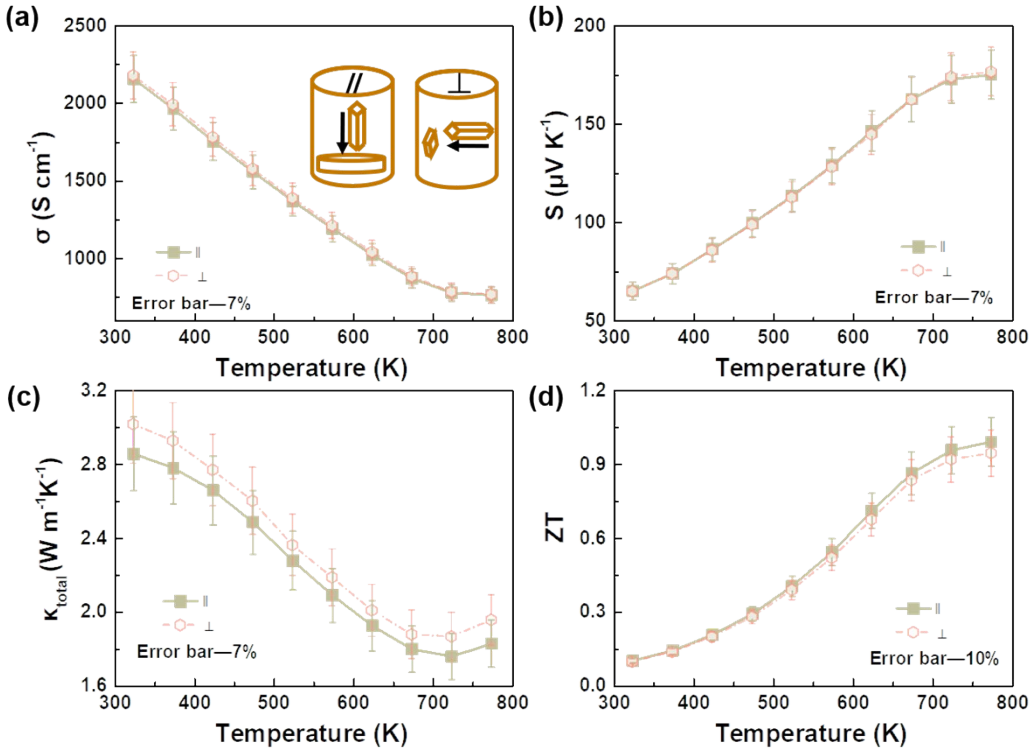

Figure S7. the temperature dependent (a) electrical conductivity, (b) Seebeck coefficient, (c) total thermal conductivity and (d) *ZT* value of $Sb_2Te_3(SnTe)_{12}$ along different directions.

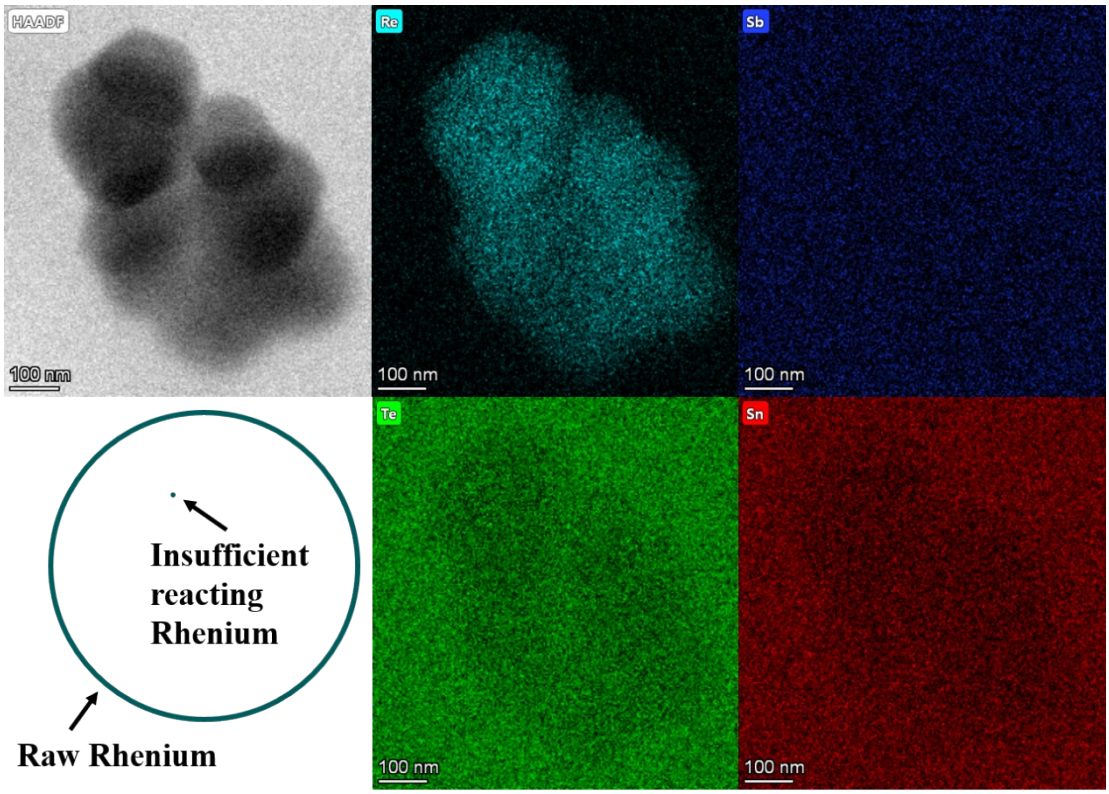

Figure S8. (a) the STEM-HAADF images of $Sb_2Te_3(Sn_{0.994}Re_{0.006}Te)_8$, (b)-(e) EDX images of the corresponding sample, and (f) the schematic diagrams of the materials before and after doping method.

Tables

Table S1. The room temperature Hall measurement value of $Sb_2Te_3(Sn_{1-x}Re_xTe)_n$ samples.

Composition (at%)	Hall coefficient ($\times10^{-9}$ m^3/C)	Carrier concentration ($\times10^{20}$ $1/cm^3$)	Mobility ($cm^2/V\cdot s$)	Conductivity (S/cm)
x=0.0	8.81	7.09	15.6	1766.78
x=0.1	8.33	7.50	15.2	1821.78
x=0.2	7.17	8.72	13.9	1932.67
x=0.4	6.23	10.0	12.5	2002.38
x=0.6	4.24	14.7	8.95	2110.04

Table. S2 The calculated cation defect formation energy of 5 different configurations of $(Sb_2Te_3)_2(SnTe)_{21}$

	$E_{tot}(V_{Sn})$ eV	E_{tot} eV	$E(Sn_{bulk})$ eV	$E^f(V_{Sn})$ eV
SnTe	-237.24	-241.95	-3.83	0.88
$(Sb_2Te_3)_3(SnTe)_{23}$-V_{Sn1}	-222.90	-227.26	-3.83	0.53
$(Sb_2Te_3)_3(SnTe)_{23}$-V_{Sn2}	-222.80	-227.26	-3.83	0.63
$(Sb_2Te_3)_3(SnTe)_{23}$-V_{Sn3}	-222.62	-227.26	-3.83	0.81
$(Sb_2Te_3)_3(SnTe)_{23}$-V_{Sn4}	-222.65	-227.26	-3.83	0.78
$(Sb_2Te_3)_3(SnTe)_{23}$-V_{Sn5}	-222.78	-227.26	-3.83	0.65
average				0.68
	$E_{tot}(V_{Sb})$ eV	E_{tot} eV	$E(Sb_{bulk})$ eV	$E^f(V_{Sb})$ eV
$(Sb_2Te_3)_3(SnTe)_{23}$-V_{Sb1}	-222.63	-227.26	-4.12	0.51
$(Sb_2Te_3)_3(SnTe)_{23}$-V_{Sb2}	-222.82	-227.26	-4.12	0.32
$(Sb_2Te_3)_3(SnTe)_{23}$-V_{Sb3}	-222.48	-227.26	-4.12	0.66
$(Sb_2Te_3)_3(SnTe)_{23}$-V_{Sb5}	-222.69	-227.26	-4.12	0.45
$(Sb_2Te_3)_3(SnTe)_{23}$-V_{Sb6}	-222.78	-227.26	-4.12	0.36
average				0.46

Table S3. Physical properties used to calculate $\kappa_{lattice}$ based on various phonon scattering processes

Parameters	**Values**
Debye temperature θ_D (K)	155[8-9]
Parameter β	2.3[8-9]
Longitudinal sound velocity υ_L(ms^{-1})	3314
Transverse sound velocity υ_T (ms^{-1})	1791
Sound velocity υ(ms^{-1})	1999
Grain size d (um)	50
Poisson's ratio V_p	0.24[8-9]
Grüneisen parameter γ	2.1[8-9]
The average lattice parameter a_{lat}	4.278
Density of gaps N_s (m^{-2})	2.7×10^{-21}

Table S4. Mass densities ρ(g/cm^3) of all samples

Compositions	ρ(g/cm^3)	Compositions	ρ(g/cm^3)
n=17	6.4279	x=0.1%	6.3983
n=14	6.4292	x=0.2%	6.3838
n=12	6.4030	x=0.4%	6.3894
n=10	6.4054	x=0.6%	6.3657
n=8	6.3983		
n=7	6.3454		

Table S5. The calculated cation defect formation energy of 4 different configurations of $Sn_{30}ReTe_{32}$

	$E_{tot}(V_{Sn})$ eV	E_{tot} eV	$E(Sn_{bulk})$ eV	$E^f(V_{Sn})$ eV
$Sn_{31}Te_{32}$	-237.28	-241.946	-3.83323	0.833207
$Sn_{30}ReTe_{32}$-1	-242.78	-246.651	-3.83323	0.037665
$Sn_{30}ReTe_{32}$-2	-242.755	-246.651	-3.83323	0.063106
$Sn_{30}ReTe_{32}$-3	-242.725	-246.651	-3.83323	0.092986
$Sn_{30}ReTe_{32}$-4	-242.733	-246.651	-3.83323	0.084499

Density functional theory (DFT) calculation

The formation energy calculations of Sn vacancy have been performed within the Vienna ab initio simulation package (VASP),[1] using the projector augmented wave (PAW) method, the Perdew-Burke-Ernzerhof (PBE) functional and the generalized gradient approximation (GGA).[2] The valence electrons of Sn, Sb and Te are $5s^25p^2$, $5s^25p^3$ and $5s^25p^4$ respectively. A plane wave cutoff energy of 350eV and a k-point density of $2\pi\times0.027$ $Å^{-1}$ using the Γ-centered Monkhorst-Pack scheme[3] were employed. A cubic 2×2×2 SnTe supercell containing 64 atoms was constructed for simulation. The special quasi-random structure (SQS) of $(Sb_2Te_3)_2(SnTe)_{21}$ (close to the ratio of $Sb_2Te_3(SnTe)_8$) was generated using the mcsqs tool as implemented in the alloy theoretic automated toolkit (ATAT).[4] The additional vacancy sites were selected randomly and an average value of formation energy was calculated for 5 configurations (Table S2). The atoms and the structures were fully relaxed until the total energy converges within 10^{-5} eV and the force converges in 0.01 eV/Å. The vacancy formation energy of Sn is defined by: $E^f(V_{Sn})=E_{tot}(V_{Sn})-E_{tot}+E(Sn_{bulk})$, where E_{tot} and $E_{tot}(V_{Sn})$ represents the total energies of the supercell before and after the introduction of an additional Sn vacancy, respectively; $E(Sn_{bulk})$ is the energy for a single Sn atom in the bulk phase.

The band structure and the density of states (DOS) of SnTe and $(Sb_2Te_3)_2(SnTe)_{21}$ were calculated within a 3×3×3 supercell containing 54 atoms. 6 Sn atoms are substituted by 4 Sb atoms and 2 vacancies randomly using ATAT. The spin-orbit coupling is included in the calculation.

Calculation of lattice thermal conductivity

To understand the phonon scattering mechanisms in this SnTe-based system, theoretical calculation based on the modified Callaway's model is carried out. According to Callaway's model, the lattice thermal conductivity is expressed as[5]:

$$k_L = \frac{k_B}{2\pi^2 v_{avg}}\left(\frac{k_B T}{\hbar}\right)^3 \int_0^{\theta_D/T} \frac{x^4 e^x}{\tau_C^{-1}(e^x-1)^2} dx \qquad \text{Equation (S1)}$$

where $x = \hbar\omega/k_B T$ is the reduced phonon frequency, w is the phonon frequency, k_B is the Boltzmann constant, $\hbar$ is the reduced Planck constant, w_D is the Debye temperature, and τ_C is the overall phonon scattering relaxation time. Five phonon scattering mechanisms are considered here, including phonon-phonon Umklapp scattering (U), Normal process (*N*), grain boundary scattering (GB), point defect scattering (PD) and gap scattering (Gap). The overall phonon scattering relaxation time is expressed as

$$\tau_C^{-1} = \tau_U^{-1} + \tau_N^{-1} + \tau_{GB}^{-1} + \tau_{PD}^{-1} + \tau_{Gap}^{-1} \qquad \text{Equation (S2)}$$

The first two contributions originate mainly from the matrix. Umklapp scattering occurs when phonons in a crystal are scattered by other phonons. Its relaxation time is of the form

$$\tau_U^{-1} = \frac{\hbar\gamma^2}{M v_s^2 \theta_D}\omega^2 T exp(-\theta_D/3T) \qquad \text{Equation (S3)}$$

where γ and M are the Gruneisen parameter, and the atomic mass, respectively. And the relaxation time for normal process is

$$\tau_N^{-1} = \beta\tau_U^{-1} \qquad \text{Equation (S4)}$$

We obtained the ratio of normal phonon scattering to Umklapp scattering, β, by fitting the lattice thermal conductivity of SnTe sample using the U+N+GB processes based on Callaway's model, shown in Figure 3(e) (red line and black plots). For common grain boundary, there is perfect acoustic mismatch at the interface between the material and vacuum, the relaxation times of phonons will be independent on the phonon frequency. The frequency-independent τ_{GB} is given by

$$\tau_{GB}^{-1} = \frac{v_s}{d} \quad \text{Equation (S5)}$$

where v_s is the average sound velocity and d is the experimentally determined grain size. Here, the average sound velocity is estimated by longitudinal and transverse sound velocity, which are measured by an ultrasonic pulse-echo method at 273 K (Table S3).

Point-defect scattering τ_{PD} arises from an atomic size disorder in alloys. The disorder is described in terms of the scattering parameter (Γ) as

$$\tau_{PD}^{-1} = \frac{V\omega^4}{4\pi {v_s}^3}\Gamma \quad \text{Equation (S6)}$$

For the pyrochlore-type solid solution $Sb_2Te_3(SnTe)_8$ sample, Sb and Sn are substituted for each other and there are three crystallographic sites, including the sites of (Sn, Sb), Te and Sn vacancy V_{Sn}, with their respective degeneracy of 10, 11, 1, respectively. And part of the vacancy in this work would generate gaps as shown in Figure 3, therefore we separately calculate the contribution of substitution, vacancy and gaps. Then[6],

$$\tau_{PD}^{-1}(Sn,Sb) = \frac{V\omega^4}{4\pi {v_s}^3}\frac{10}{22}\left(\frac{M_{(Sn,Sb)}}{\overline{M}}\right)^2\Gamma_{(Sn,Sb)} \quad \text{Equation (S7)}$$

$$\Gamma_{(Sn,Sb)} = 0.2 * 0.8\left[\left(\Delta M/M_{(Sn,Sb)}\right)^2 + \varepsilon\left(\Delta\delta/\delta_{(Sn,Sb)}\right)^2\right] \quad \text{Equation (S8)}$$

where

$$\Delta M = M_{Sn} - M_{Sb} \quad \text{Equation (S9)}$$

$$\Delta\delta = \delta_{Sn} - \delta_{Sb} \quad \text{Equation (S10)}$$

$$M_{(Sn,Sb)} = 0.2 * M_{Sn} + 0.8 * M_{Sb} \quad \text{Equation (S11)}$$

$$\delta_{(Sn,Sb)} = 0.2 * \delta_{Sn} + 0.8 * \delta_{Sb} \quad \text{Equation (S12)}$$

$$\varepsilon = \frac{2}{9}\left[\frac{6.4\gamma(1+V_p)}{1-V_p}\right]^2 \quad \text{Equation (S13)}$$

Where $M_{(Sn,Sb)}$ is the average mass of the (Sn, Sb) sites and $\overline{M}$ is the average mass of $Sb_2Te_3(SnTe)_8$ sample. V_p is the Poisson's ratio, δ is the radius of atoms.

$$\tau_{PD}^{-1}(V_{Sn}) = \frac{V\omega^4}{4\pi v_s^3} \frac{1}{22} \left(\frac{M_{(Sn,\,Sb)}}{\overline{M}}\right)^2 \Gamma_{(V_{Sn})} \qquad \text{Equation (S14)}$$

$$\Gamma_{(V_{Sn})} = \frac{10}{11 * 11}\left[\left(M_{Sn}/M_{(Sn,\,Sb)}\right)^2 + \varepsilon\left(\delta_{Sn}/\delta_{(Sn,\,Sb)}\right)^2\right] \qquad \text{Equation (S15)}$$

The gap in this work is recognized as stacking fault, which can be expressed as, [7]

$$\tau_{SF}^{-1} = 0.7\frac{a_{lat}^2 \gamma^2 N_s}{v_s}\omega^2 \qquad \text{Equation (S16)}$$

Here, τ_{SF} represents τ_{gap} and a_{lat}, γ, N_s, v_s *and* ω are the average lattice parameter, Grüneisen parameter, density of gaps, sound speed and frequency, respectively. All the calculated parameters could be found in the Table S3.

Predicting the number density of vacancies from the starting composition

Firstly, suppose that the size of the planar defects is as 35×35 nm^2. A line profile result from our TEM observations presented that every 10 vacancies deserved ~3.5 nm, indicating that there are ~10^4 vacancies in this area of 35×35 nm^2.

Secondly, according to our XRD results, $Sb_2Te_3(SnTe)_8$ has the same lattice matrix with SnTe, thus, there are 4 SnTe in a unit cell (a ~ 0.6 nm), which means 4/11 vacancies in a $Sb_2Te_3(SnTe)_8$ unit cell. Therefore, the volume of 10^4 vacancies in the $Sb_2Te_3(SnTe)_8$ can be calculated as $a^3*10^4/(4/11)$.

Thirdly, the characteristic length between two gaps can be calculated as volume/area ~ 4.85 nm (depicted in Figure S2(d)).

References

1. G. Kresse, J. Furthmüller, *Phys. Rev. B.* 1996, **54**, 11169.
2. J. P. Perdew, K. Burke, M. Q. Hao, H. Chi, T. P. Bailey, L. D. Zhao, C. Uher, C. Wolverton, V. P. Dravid, M. Ernzerhof, *Phys. Rev. Lett.* 1996, **77**, 3865.
3. H. J. Monkhorst, J. D. Pack, *Phys. Rev. B.* 1976, **13**, 5188.
4. A. Zunger, S.H. Wei, L. G. Ferreira, J. E. Bernard, *Phys. Rev. Lett.* 1990, **65**, 353.
5. B. Zhu, Z. Y. Huang, X. Y. Wang, Y. Yu, L. Yang, N. Gao, Z. G. Chen, F. Q. Zu, *Nano Energy.* 2017, **42**, 8.
6. C. L. Wan, W. Pan, Q. Xu, Y. X. Qin, J. D. Wang, Z. X. Qu and M. H. Fang, *Phys. Rev. B.* 2006, **74**, 144109.
7. B. K. Singh, V. J. Menon and K. C. Sood, *Phys. Rev. B.* 2006, **74**, 184302.
8. X. Zhang, D. Wang, H. Wu, M. Yin, Y. Pei, S. Gong, L. Huang, S. J. Pennycook, J. He, L. D. Zhao, *Energy Environ. Sci.* 2017, **10**, 2420.
9. C. Toher, J. J. Plata, O. Levy, M. de Jong, M. Asta, M. B. Nardelli, S. Curtarolo, *Phys. Rev. B.* 2014, **90**, 174107.